B. Geppert*, D. Groeneveld, M. Bittner and A. Feldhoff

Experimental Characterisation and Finite-element Simulations of a Thermoelectric Generator with Ceramic p-type $Ca_3Co_4O_9$ and Metallic n-type $Cu_{0.57}Ni_{0.42}Mn_{0.01}$ Legs

DOI 10.1515/ehs-2016-0022

Abstract: This study presents the characterisation of a prototype thermoelectric generator including ceramic $Ca_3Co_4O_9$ p-type and metallic $Cu_{0.57}Ni_{0.42}Mn_{0.01}$ n-type legs. The generator was constructed applying the conventional rigid chessboard design, which provides an electrical series connection of the thermoelectrically active materials in between of two electrical isolating cover plates made of alumina. Ag-epoxy resin was used for electric connectors which were directly bond to the thermoelectrically active materials. The generator was rebuild in the framework of a finite-element model to simulate the generator's transport characteristics using the physical data of the single materials as input parameters for the simulation tool. The simulation results give a view to the distributions of temperature and electric potential as well as vector plots showing the generated current density of charge inside the regarded materials. The finite-element simulation tool was used to consider the electrical contact resistivities between the thermoelectric legs and the connector material. The input parameter for the specific isothermal electric resistivity of the Ag-epoxy connectors were varied by including the electrical contact resistances to match the simulated to the measured data in order to receive the correct electric current densities in the modeled device.

Keywords: thermoelectric generator, finite-element simulation, electrical power

Introduction

The development and application of thermoelectric materials, for example, for harvesting electrical power from waste heat sources, is a current field of study that requires interdisciplinary investigations. The implementation of newly developed thermoelectric materials into thermoelectric generators (TEGs) benefits from modeling the thermoelectric properties of the generators with respect to the individual properties of the employed materials. A TEG is a device that transfers energy from thermal (entropy) current to electric current; see Fuchs (2010, 2014) and Feldhoff (2015). The concept of energy carriers as outlined by Falk, Herrmann, and Schmid (1983) enables an elegant description of a thermoelectric device, which relies on considering the flux densities of the aforementioned fluid-like quantities entropy S and electric charge q and their linkage to the conjugated potentials, which are the absolute temperature T and the electric potential φ, respectively. The currents of thermal energy (heat) and electric energy are then obtained as shown by Fuchs (2014), Feldhoff and Geppert (2014a, 2014b) and Feldhoff (2015). Taking the cross-sectional areas A_{leg} and the length L_{leg} of the thermoelectric material samples into account, the currents of entropy I_S and electric charge I_q in a thermoelectric material, that is subjected to differences of thermal potential ΔT and electric potential $\Delta\varphi$, can be easily obtained if a thermoelectric material tensor is considered; see Feldhoff (2015):

$$\begin{pmatrix} I_S \\ I_q \end{pmatrix} = -\frac{A_{leg}}{L_{leg}} \cdot \begin{pmatrix} \sigma \cdot \alpha^2 + \Lambda & \sigma \cdot \alpha \\ \sigma \cdot \alpha & \sigma \end{pmatrix} \cdot \begin{pmatrix} \Delta T \\ \Delta\varphi \end{pmatrix} \quad (1)$$

The thermoelectric tensor consists of three tensorial quantities, the specific electrical conductivity σ under isothermal conditions (i. e., $\nabla T = 0$), the specific entropy conductivity Λ under electric open-circuited conditions (i. e., $I_q = 0$) and the Seebeck coefficient α. Special cases that can be received under certain conditions of eq. (1) were elucidated by Fuchs (2014), Feldhoff and Geppert (2014a, 2014b) and Feldhoff (2015).

The basic unit of a thermoelectric generator can be constructed by connecting two materials with different algebraic signs for the Seebeck coefficient α thermally in parallel and electrically in series. For $\alpha < 0$, the motions of thermal and electrical fluxes are directed in the same

***Corresponding author: B. Geppert,** Institute of Physical Chemistry and Electrochemistry, Leibniz Universität Hannover, Hannover, Germany, E-mail: benjamin.geppert@pci.uni-hannover.de
D. Groeneveld, M. Bittner, A. Feldhoff, Institute of Physical Chemistry and Electrochemistry, Leibniz Universität Hannover, Hannover, Germany

way. In contrast, for $\alpha > 0$, the thermal and electrical fluxes are directed in opposite directions; see Feldhoff and Geppert (2014b). By additively connecting several of these basic units thermally in parallel and electrically in series, the electric potential φ can be increased over the device; see Feldhoff (2015) for illustration. The choice of the thermoelectric materials that comprise the TEG depends on the conditions under which the energy conversion is to be performed.

Among the various thermoelectric materials, semiconductors exhibit the best thermoelectric conversion efficiency because of their moderate charge carrier concentration, and they provide a good balance between specific electric conductivity σ, the Seebeck coefficient α and the thermal conductivity; see Ioffe (1957). Alloys provide high values of the so-called power factor $\sigma \cdot \alpha^2$, which is the charge-coupled entropy conductivity and occurs as part of the thermoelectric tensor in eq. (1). Consequently, alloys and semiconductors are chosen as thermoelectrically active materials. To obtain a good TEG performance, the combination of n- and p-type materials and a low-resistance electrical connection between them realized by metals or alloys is preferred. In case of the present study, a composite connector material, Ag-epoxy resin, was used.

Additionally, the geometric properties of the materials that are combined to form the complete device have to be optimized for every system. Finite-element method (FEM) simulations are useful for calculating the thermoelectric performance in terms of the used materials and their geometric properties without constructing a real TEG. The thermoelectric properties can be measured for each individual material. Afterwards, the materials can be combined in a simulated TEG system with a specific geometry. The absolute currents I are correlated to the current densities j considering the cross-sectional areas of the thermoelectric material legs A_{leg}, as shown in eqs (2) and (3).

$$I_S = A_{leg} \cdot j_S \tag{2}$$

$$I_q = A_{leg} \cdot j_q \tag{3}$$

Under electric open-circuit conditions, eq. (1) yields the entropy current I_S through the thermoelectric material by Fourier's law:

$$I_S = -\frac{A_{leg}}{L_{leg}} \cdot \Lambda \cdot \Delta T \tag{4}$$

The specific entropy conductivity Λ is related to the specific heat conductivity λ by the absolute working temperature T, see Fuchs (2010, 2014) and Feldhoff (2015).

$$\lambda = T \cdot \Lambda \tag{5}$$

Under isothermal conditions, eq. (1) yields the electric current I_q through the thermoelectric material by Ohm's law:

$$I_q = -\frac{A_{leg}}{L_{leg}} \cdot \sigma \cdot \Delta\varphi \tag{6}$$

Experimental

Thermoelectric Measurement Setup

To characterize the thermoelectric properties of the materials, the temperature-dependent isothermal specific electric resistivity and the Seebeck coefficient, as estimated from the thermovoltage, were measured. A precision vertical diamond wire-saw model 3242 from O'WELL was used for sample preparation. Thermoelectric properties were measured using a measurement cell constructed in-house. The sample was clamped between two platinum electrodes to close the electric circuit in a pseudo-four-point measurement. The applied furnace was an ELITE thermal system. The Seebeck coefficient was measured using a NORECS Probostat measurement system. The electronic parameters were measured with KEITHLEY 2100 $6\frac{1}{2}$ digit multimeters. The measured data were converted using LAB VIEW software.

To estimate the thermoelectric characteristics of the constructed TEG, it was placed between a heat source (ceramic hot-plate) and a heat sink (passive cooler). A photomicrograph of the measurement setup is shown in Figure 1.

The temperature data were collected using thermocouples. The voltage $\Delta\varphi$ was measured as the drop of the electric potential on the external load R_{load}. The electric output power P_{el} was estimated according to:

$$P_{el} = I_q \cdot \Delta\varphi \tag{7}$$

The resistivity of the thermoelectric generator was estimated by analysing the electric current-voltage characteristics using Ohm's law for the entire device (see eq. (6) for the corresponding relation for single materials).

$$\Delta\varphi = -R_{TEG} \cdot I_q \tag{8}$$

The geometric parameters of applied materials, that are input parameters for the FEM tool, are listed in Table 1.

Microstructure Analysis

The phase composition of the metallic n-type and ceramic p-type materials was analyzed by X-ray diffraction (XRD)

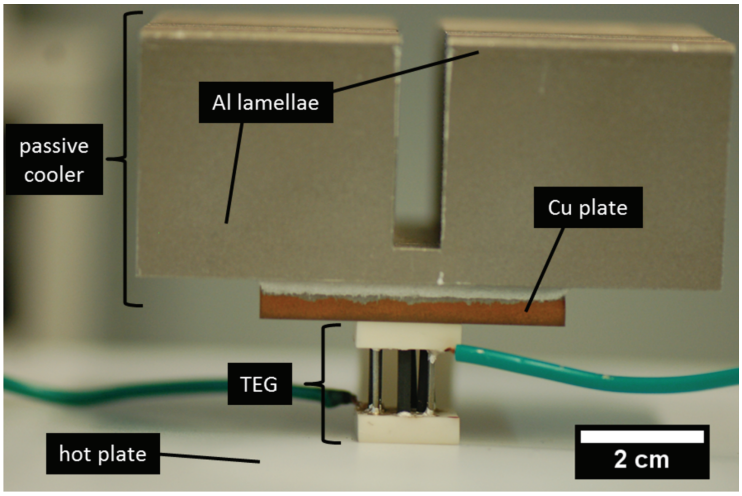

Figure 1: Photomicrograph of the measurement setup for determination of the thermoelectric characteristics of the constructed TEG. Note that the p-type ceramic material is integrated as rectangular bars while the n-type wire material exhibits the form of a cylinder.

Table 1: Measured geometric properties of the TEG's components: length L and cross-sectional area A of applied material. The fill-factor of the TEG exhibits a value of 7.5 %.

Component	Material	L/mm	A/mm^2	Description
p-type leg	$Ca_3Co_4O_9$	10.0	3.23	House-made ceramic
n-type leg	$Cu_{0.57}Ni_{0.42}Mn_{0.01}$	10.0	0.79	Commercial alloy
el. connector	Ag-epoxy resin	0.44	5.32	Commercial composite
Cover plates	Al_2O_3	3.8	225	Commercial ceramic

using a Bruker D8 Advance with Cu-K_α radiation. The thermoelectric bulk materials were polished using diamond-lapping films (Allied High Tech Multiprep) for field-emission scanning electron microscopy (FE-SEM) investigations using a JEOL JSM-6700F, which was equipped with an Oxford Instruments INCA 300 energy-dispersive X-ray spectrometer (EDXS) for elemental analysis.

Materials Choice

The p-type leg material was realized by applying ceramic $Ca_3Co_4O_9$. This layered cobaltite phase exhibits an incommensurate structure and provides attractive thermoelectric properties, see Lambert, Leligny, and Gebrille (2001). Measured thermoelectric parameters for polycrystalline samples from various laboratories were assembled by Fergus (2011). Single crystals of $Ca_3Co_4O_9$ exhibit a figure of merit $ZT = 0.83$ at 973 K, see Shikano and Funahashi (2003). The high charge carrier density around room temperature makes the $Ca_3Co_4O_9$ ceramic also usable as thermoelectric material for low- and intermediate-temperature devices. As n-type material a Cu-Ni based alloy was used. For energy conversion in the intermediate temperature range such metallic compounds show useful properties. The electric resistance is very low and the value for the Seebeck coefficent is acceptable. That makes such alloys the material class reaching highest values of the power factor. We already used this material combination for the construction of flexible thermoelectric generators, see Geppert and Feldhoff (2015). Measured thermoelectric properties were summarized in round-robin measurements and reported by Lu et al. (2009) and Lowhorn et al. (2009).

The series connection of n- and p-type legs of the generator was realized using Ag-epoxy resin as electrical conductive glue. The bulk resistivity was reported with a value of 0.9 mΩcm^{-1}.

For the cover plates, commonly used Al_2O_3 was applied.

Finite-element Simulations

In this work, a prototype thermoelectric generator was constructed and rebuild in the FEM tool using ANSYS Mechanical APDL version 15.0 academic. The specific resistivity of the Ag-epoxy resin was adapted in the simulation to match the measured transport properties and to obtain the correct electric currents in the modeled device. The model consists of 14,268 elements. Each thermoelectric p-type leg is build up by 48 elements (total number of p-type material elements for the thermoelectric legs is

192) while the total number of elements for the electrical Ag-epoxy connectors is 2964. Each alumina cover plate consists of 1482 elements. The simulation procedure was performed using the 3-D steady-state thermoelectric analyser. The residual method was done using the thermal power P_{th} and electric current I_q as convergence parameters. The convergence values were set to $1 \cdot 10^{-3}$ for both parameters. The entire fit function is presented in eq. (9).

$$P_{th} = \alpha_{TEG} \cdot T_h \cdot I_q - \frac{1}{2} \cdot I_q^2 \cdot R_{TEG} + \lambda \cdot \Delta T \tag{9}$$

The non-linear solution converged after 5 equilibrium iterations. The constructed and modeled device is presented in Figure 2.

Results and Discussion

Microstructure of Materials

The crystallographic phases of the sintered p-type $Ca_3Co_4O_9$ ceramic and the n-type $Cu_{0.57}Ni_{0.42}Mn_{0.01}$ were confirmed by Rietveld refinement of measured X-ray diffractograms. The diffractograms (blue curves) of the thermoelectric materials are presented in Figure 3 together with the Rietveld fits (red curves). $Ca_3Co_4O_9$ crystallizes in the monoclinic system and exhibits the *Cm* symmetry for both subsystems (b_1, b_2). $Cu_{0.57}Ni_{0.42}Mn_{0.01}$ crystallizes in the cubic system exhibiting the spacegroup $Fm\bar{3}m$.

The p-type $Ca_3Co_4O_9$ ceramic was vibration-polished to estimate the arrangement of plate-like grains inside the bulk material. In Figure 4, a secondary electron micrograph of the ceramic material is presented. The black areas are internal pores.

Thermoelectric Investigations

Table 2 lists measured or reported values for the transport properties of each material that was applied in the generator. The electronic and thermal quantities for the Al_2O_3 plates and for the Ag-epoxy resin were taken from manufacturers data.

To estimate the thermoelectric properties of the TEG, the device was characterized in the setup shown in Figure 1. The temperature-dependent resistivity of the entire device R_{TEG} was estimated by applying Ohm's law (eq. (8)) to the TEG's measurement data. In Table 3, the

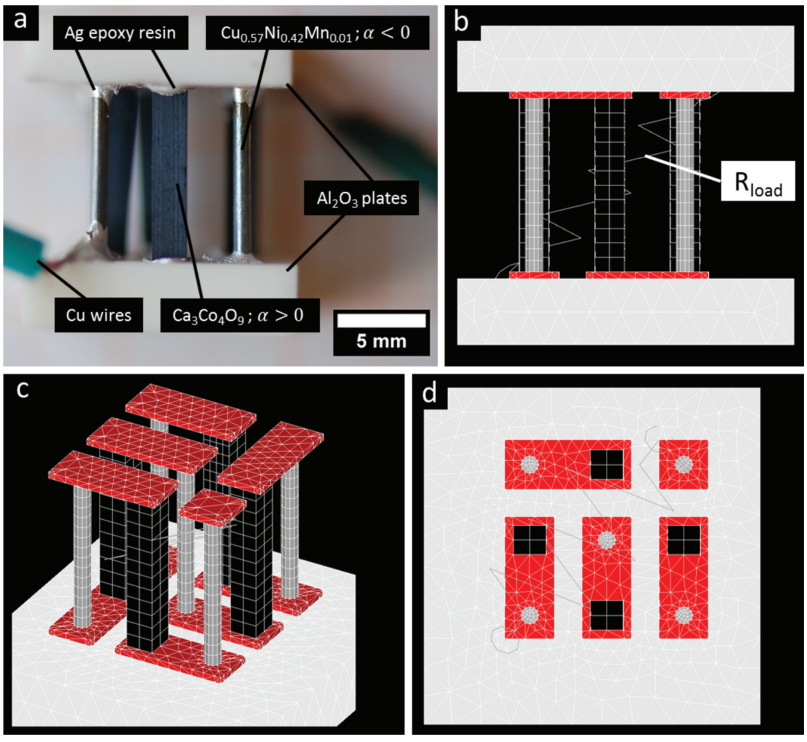

Figure 2: View on the constructed and modeled thermoelectric device. (a) Side-view of constructed TEG, (b) Side-view of modeled device, (c) Perspective view of modeled device, (d) Top-view on modeled device.

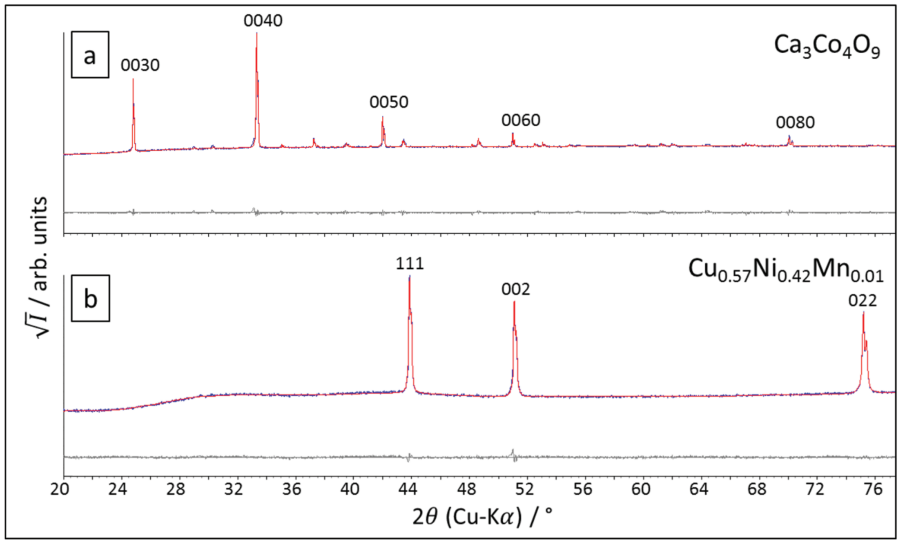

Figure 3: Measured X-ray diffractograms (blue curves) with Rietveld fits (red curves) and differential curve (grey curves). (a) p-type $Ca_3Co_4O_9$ ceramic, (b) n-type $Cu_{0.57}Ni_{0.42}Mn_{0.01}$ alloy. The counts are presented as square-root values.

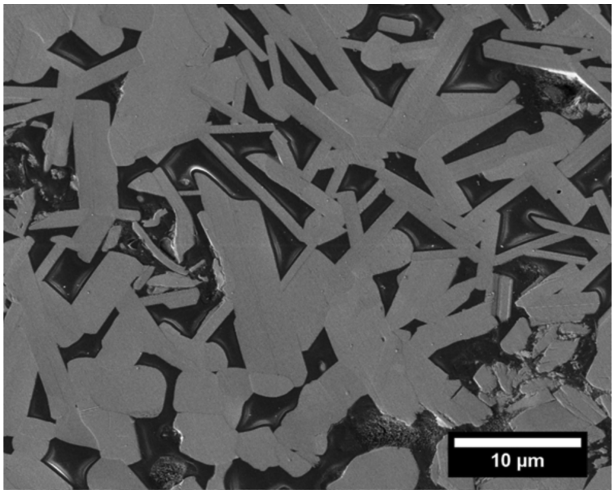

Figure 4: Secondary electron micrograph of the vibration-polished p-type $Ca_3Co_4O_9$ ceramic material.

values for the determined contact resistances are listed together with the maximum electric current $I_{q,SC}$ under electric short-circuit conditions (i. e. $\Delta\varphi = 0$), the open-circuit voltage $\Delta\varphi_{OC}$ (i. e. $I_q = 0$) and the maximum electric output power $P_{el,max}$. All quantities are related to the established temperature drops ΔT and the median temperature of the device T_{median}.

The FEM simulation resulted in accurate values for the open-circuit voltage $\Delta\varphi_{OC}$ (device Seebeck-voltage) but in too high values for the short-circuit electric current $I_{q,SC}$. This makes the calculated values for the resistivity of the generator too low and the electric output power too high. The reason for the FEM solutions to be inaccurate is seen in contact resistivities between the Ag-epoxy resin and the thermoelectrically active materials. In order to match the characteristics of the real constructed TEG to the modeled device in the FEM tool, the specific electric resistivity of the Ag-epoxy resin was refined by the implementation of the magnitude of the contact resistances into the values of the specific resistivity of the connector material. The values of the resistivity of the electric connector material was varied until the Ohm-lines of the FEM simulation fitted the measurement data points. In the framework of thermoelectric generator fabrication the formation of contact resistances is a major concern and affects the thermoelectric properties of a certain device on a large scale. The modification of interfaces in thermoelectric generators is an extensive field of study. LeBlanc (2014) compared material and generator efficiency and he showed that the efficiency can decrease up to 59% comparing the single thermoelectric materials and the entire assembled systems. The $Ca_3Co_4O_9$-related oxide-metal interfaces were studied by Holgate et al. (2014).

Figure 5(a) shows $\Delta\varphi - I_q$ curves with bad agreement of the FEM Simulation A, that does not consider the electrical contact resistances (dotted lines), and good agreement of the FEM Simulation B, that does consider the electrical contact resistances (solid lines), with the measurement (data points) for all temperature conditions. Note, that the absolute value of the slope of the lines refers to the internal resistance R_{TEG}, as indicated in

Table 2: Determined or reported thermoelectrical parameters of applied materials. Simulation A assumes vanishing contact resistances and Simulation B accounts for non-vanishing contact resistances by considering them by varying the effective resistance ρ of the connector material.

Material	T/K	ρ/m$\Omega \cdot$ cm	$\alpha/\mu V \cdot K^{-1}$	$\lambda/W \cdot m^{-1} \cdot K^{-1}$	$\Lambda/W \cdot m^{-1} \cdot K^{-2}$
$Ca_3Co_4O_9$	363	59.21	147.39	0.62	$1.7 \cdot 10^{-3}$
	403	49.93	154.95	0.59	$1.5 \cdot 10^{-3}$
	443	36.58	162.53	0.57	$1.3 \cdot 10^{-3}$
	478	32.66	169.12	0.57	$1.2 \cdot 10^{-3}$
$Cu_{0.57}Ni_{0.42}Mn_{0.01}$	300–500	$4.7 \cdot 10^{-2}$	-40	23	$7.7 \cdot 10^{-2}$
Al_2O_3 plates	300	$1 \cdot 10^{17}$	n.a.	30	$1 \cdot 10^{-1}$
Ag-epoxy resin	300	0.9	n.a.	1	$3.3 \cdot 10^{-3}$
(Simulation A)					
Ag-epoxy resin	363	$2.55 \cdot 10^{3}$	n.a.	1	$2.8 \cdot 10^{-3}$
(Simulation B)	403	$1.65 \cdot 10^{3}$	n.a.	1	$2.5 \cdot 10^{-3}$
	443	$5.10 \cdot 10^{2}$	n.a.	1	$2.3 \cdot 10^{-3}$
	478	$4.30 \cdot 10^{2}$	n.a.	1	$2.1 \cdot 10^{-3}$

Table 3: Estimated thermoelectric parameters of the constructed TEG for different temperature conditions.

T_{hot}/K	ΔT/K	T_{median}/K	R_{TEG}/Ω	$P_{el,max}/\mu W$	$\Delta\varphi_{OC}$/mV	$I_{q,SC}$/mA	$R_{contact}/\Omega$ per contact
389	60	363	415.24	0.93	39.4	0.09	22.66
441	80	403	250.36	2.90	53.9	0.22	19.12
492	100	443	74.50	16.54	70.2	0.94	3.89
536	120	478	63.93	32.52	91.2	1.43	3.33

Tables 3 and 4. The electric output power P_{el} was estimated in terms of different load resistivities R_{load}. The electrical contact resistances limit the magnitude of the electric current inside the device and therefore the electric power output. Deviations of simualtion B and the measurement data are probably caused by the applied approximations. The electrical contact resistances were assumed to be identical at each junction. Due to the usage of different material classes such an approach is very rude and causes slightly inaccurate values for the internal load R_{TEG}. The power characteristics of measured data and FEM results are displayed in Figure 5(b). The results of simulation A are highly overestimated. For simulation B and the measurement data, the characteristic power-plots show a comparable curvature. For decreasing temperature, the measured electric current deviates more and more from the values of simulation B. This simulation concerns the electric contact resistances but thermal contact resistances were neglected. Therefore, the thermal current densities inside the simulated materials are not absolutely correct. Such a lack of accuracy for the values of the thermal power P_{th} can cause deviations in the solutions for the electric power output P_{el} because these quantities depend on each other at constant thermoelectric conversion efficieny η_{TE}. The relation is given in eq. (10).

$$P_{el} = \eta_{TE} \cdot P_{th} \tag{10}$$

For absolutely correct solutions of FEM simulations in the framework of thermoelecric generator performance, both, the electric and the thermal contact resistances have to be considered, see Högblom and Andersson (2014). Implementation of contact resistances (electrical and thermal) into FEM simulations is not straight forward (see Annapragada et al. (2012)).

The simulation results are presented as contour-plots for the potential distributions and as vectorial plots that refer to the density of electric current j_q in simulation A and simulation B. The colors of the vectors refer to the local value of the flux density of the transported quantity, which is indicated in the legend. Figure 6(a) shows the distribution of the entropy potential T, obtained from the FEM simulation and a perspective view of the TEG at maximum electric power output for a potential drop of $\Delta T = 120$K. The situation of temperature distribution is equal for

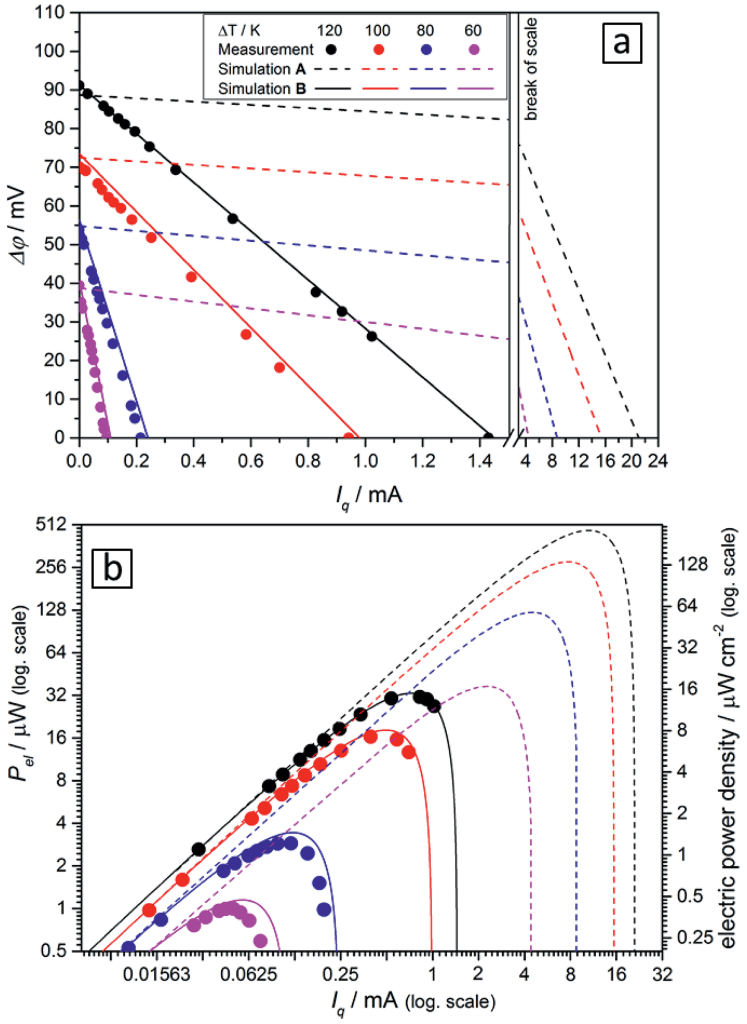

Figure 5: Measured (dots) and simulated (lines) results for the thermoelectric characteristics of the constructed TEG. (a) Electric voltage-current $\Delta\varphi$-I_q characteristics of the measured data and the FEM simulation A (dashed lines) and simulation B (solid lines), (b) Electric power-current P_{el}-I_q characteristics for measured data and the FEM simulation A and B. For better comparison, the values are plotted logarithmically.

Table 4: Thermoelectric parameters of the modeled TEG for Simulation A and Simulation B.

			Simulation A				Simulation B			
T_{hot}/K	ΔT/K	T_{median}/K	R_{TEG}/Ω	$P_{el,max}$/µW	$\Delta\varphi_{OC}$/mV	$I_{q,SC}$/mA	R_{TEG}/Ω	$P_{el,max}$/µW	$\Delta\varphi_{OC}$/mV	$I_{q,SC}$/mA
389	60	363	7.33	37.01	40.4	5.32	355.85	1.15	40.5	0.11
441	80	403	6.11	123.31	53.9	8.82	231.66	3.43	56.4	0.24
492	100	443	4.53	280.01	73.3	15.3	74.31	18.17	73.5	0.98
536	120	478	4.04	467.13	91.0	21.1	62.89	33.12	91.3	1.45

simulations A and B. Figure 6(b) shows the respective distribution of the electric potential $\Delta\varphi$ along the electrical serial connection of the assembled thermoelectric legs and electric connectors (Ag-epoxy resin) inside the thermoelectric generator. The displayed simulation results of the TEG are related to the conditions of electric power maximum (from Figure 5(b)) for a temperature drop of 120 K.

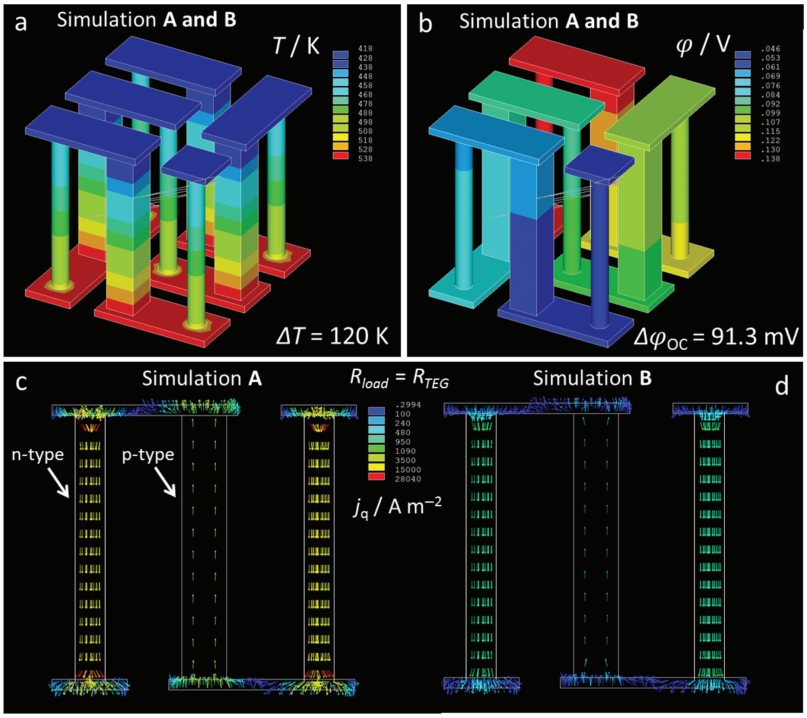

Figure 6: Simulated results for the thermoelectric characteristics of the constructed TEG. (a) Temperature distribution for $\Delta T = 120K$ for simulation A and B, (b) distribution of electric potential along the electric series connection of TE legs for electric open-circuit conditions (nearly equal values for simulation A and B), (c) electric current density j_q for simulation A, (d) electric current density j_q for simulation B. Note that the current densities for simulation A and simulation B are correlated to the same color-related legend and refer to electric maximum power condition. For comparison of temperature related quantities see Table 4.

The flux density of electric charge j_q depends on the material of the TEG's components and on the local potential gradients according to the potential distributions shown in Figure 6(a) and (b). The modeling of TEGs using the FEM method has the advantage of providing deep insight into the distribution of all relevant quantities throughout the entire device. From Figure 6(c) and (d), it is obvious that the electric current density j_q inside the entire arrangement of materials is much smaller than predicted by simulation A. Therefore, the electric power output predicted by simulation A is more than 10 times higher compared to the electric power received by simulation B and the experiment. In the metallic $Cu_{0.57}Ni_{0.42}Mn_{0.01}$ legs the electric current density is more than 3 times lower in simulation B compared to the results of simulation A. Varying the specific electric resistivity of the electric connector Ag-epoxy resin, by taking the contact resistances into account, results in almost correct densities of electric current inside each material. The contact region of the Ag-epoxy resin and the thermoelectric materials limits the electric current density inside the entire generator because electric contact resistances between the connector material and the thermoelectric legs are formed. The results from the finite-element simulation illustrate the relation between the entropy potential T and electric potential φ, which is given algebraically in eq. (1) by the respective distribution of potentials, and the obtained electric current I_q.

Summary and Conclusions

The model thermoelectric system created from the finite-element simulation provides results with acceptable accuracy in terms of the values for the open-circuit voltages. The simulation for the current densities and therefore for the electric power output of the generator was predicted with too high values. The overestimation of the electric current density is based on the formation of contact resistivities that were formed at the material boundaries of the Ag-epoxy resin as electric connector and the thermoelectrically active materials. Those contacts in TEG devices can be realized by different materials. The Ag-epoxy resin exhibits good properties in terms of processibility and mechanical fixation. The adhesive is more heat proved than Sn-Pb based solders. However, the

contact resistances in thermoelectric generators are an important concern. Using the finite-element simulation tool, the quantitative electrical contact resistances could be determined.

After including the contact resistances into the electric resistivities of the connector material a good match of measured and simulated data were obtained. The Ag-epoxy resin was used as an alternative to soldering that can also exhibit high contact resistivities when ceramic materials are applied. The used thermoelectric materials are p-type $Ca_3Co_4O_9$ ceramic and n-type $Cu_{0.57}Ni_{0.42}Mn_{0.01}$ alloy. The FEM simulation was used to estimate the limiting factor in terms of electric power output. The theoretical maximum power was calculated to almost 500 μW with a temperature difference of $\Delta T = 120$ K, while the measured maximum electric power output for the same temperature conditions was only 32.5 μW. The FEM results show that a minimization of the contact resistances in TEG devices can dramatically increase the electric output power. At lower temperatures the $Ca_3Co_4O_9$ ceramic provides a charge carrier density that is usable also in devices for low-temperature applications. Deep insights into the local variations of the relevant thermoelectric parameters can be obtained from this type of FEM modeling. Overall, the developed model system can predict the thermoelectric properties of a certain TEG quite well if the proper parameters for feeding the simulation tool are selected. Work on thermoelectric materials and systems benefits from the use of FEM simulations to compare the properties of the modeled and the measured device to gain knowledge on the factors that limit the electric power output of a certain thermoelectric generator.

References

Annapragada, S., T. Salamon, P. Kolodner, M. Hodes, and S. Garimella. 2012. "Determination of Electrical Contact Resistivity in Thermoelectric Modules (TEMs) from Module-Level Measurements." *Transactions on Components, Packaging and Manufactering Technology* 2 (4):668–676.

Falk, G., F. Herrmann, and G. Schmid. 1983. "Energy Forms or Energy Carriers?." *American Journal Physical* 51:1074–1077.

Feldhoff, A. 2015. "Thermoelectric Material Tensor Derived from the Onsager – De Groot – Callen Model." *Energy Harvesting and Systems* 2 (1–2):5–13.

Feldhoff, A., and B. Geppert. 2014a. "Erratum to EHS 1 (1-2), 69-78 (2014): A High-Temperature Thermoelectric Generator Based on Oxides." *Energy Harvesting and Systems* 1 (3–4):251.

Feldhoff, A., and B. Geppert. 2014b. "A High-Temperature Thermoelectric Generator Based on Oxides." *Energy Harvesting and Systems* 1 (1–2):69–78.

Fergus, J. 2011. "Oxide Materials for High Temperature Thermoelectric Energy Conversion." *Journal of the European Ceramic Society* 32:525–540.

Fuchs, H. 2010. *The Dynamics of Heat – A Unified Aproach to Thermodynamics and Heat Transfer*, Graduate Texts in Physics, 2nd ed. New York: Springer.

Fuchs, H. 2014. "A Direct Entropic Approach to Uniform and Spatially Continuous Dynamical Models of Thermoelectric Devices." *Energy Harvesting and Systems* 1 (3–4):253–265.

Geppert, B., and A. Feldhoff. 2015. "An Approach to a Flexible Thermoelectric Generator Fabricated Using Bulk Materials." *Energy Harvesting and Systems* 2:1–11.

Högblom, O., and R. Andersson. 2014. "Analysis of Thermoelectric Generator Performance by Use of Simulations and Experiments." *Journal of Electronic Materials* 46 (6):2247–2254.

Holgate, T., L. Han, N. Wu, E. Bojesen, M. Christensen, B. Iversen, N. Nong, and N. Pryds. 2014. "Characterisation of the Interface between an Fe-Cr Alloy and the P-Type Thermoelectric Oxide $Ca_3Co_4O_9$." *Journal of Alloys and Compounds* 585:827–833.

Ioffe, A. 1957. *Semiconductor Thermoelements and Thermoelectric Cooling*, 1st ed. London: Infosearch Ltd.

Lambert, S., H. Leligny, and D. Gebrille. 2001. "Three Forms of the Misfit Layered Cobaltite $[Ca_2CoO_3]$ $[CoO_2]_{1.62}$ · A 4D Structural Investigation." *Journal of Solid State Chemistry* 160:322–331.

LeBlanc, S. 2014. "Thermoelectric Generators: Linking Material Properties and Systems Engineering for Waste Heat Recovery Applications." *Sustainable Materials and Technologies* 1–2:26–35.

Lowhorn, N.D., W. Wong-Ng, W. Zhang, Z.Q. Lu, M. Otani, E. Thomas, M.G.T.N. Tran, N. Dilly, S. Ghamaty, N. Elsner, T. Hogan, A.D. Downey, Q. Jie, Q. Li, H. Obara, J. Sharp, C. Caylor, R. Venkatasubramanian, R. Willigan, J. Yang, J. Martin, G. Nolas, B. Edwards, and T. Tritt. 2009. "Round-Robin Measurements of Two Candidate Materials for a Seebeck Coefficient Standard Reference Material." *Applied Physics A* 94:231–234.

Lu, Z.Q.J., N.D. Lowhorn, W. Wong-Ng, W. Zhang, Z.Q. Lu, M. Otani, E. Thomas, M.G.T.N. Tran, N. Dilly, S. Ghamaty, N. Elsner, T. Hogan, A.D. Downey, Q. Jie, Q. Li, H. Obara, J. Sharp, C. Caylor, R. Venkatasubramanian, R. Willigan, J. Yang, J. Martin, G. Nolas, B. Edwards, and T. Tritt. 2009. "Statistical Analysis of a Round-Robin Measurement Survey of Two Candidate Materials for a Seebeck Coefficient Standard Reference Material." *Journal of Research of the National Institute of Standards and Technology* 114:37–55.

Shikano, M., and R. Funahashi. 2003. "Electrical and Thermal Properties of Single-Crystalline $(Ca_2CoO_3)_{0.7}CoO_2$ with a $Ca_3Co_4O_9$ Structure." *Applied Physics Letter* 82 (12):1851–1851.